

# Supporting Information: Dihydrogen vs Hydrogen Bonding in the Solvation of Ammonia Borane by Tetrahydrofuran and Liquid Ammonia

David Ingram,<sup>a,b</sup> Thomas Headen,<sup>\*c</sup> Neal Skipper,<sup>a,d</sup>  
Samantha Callear,<sup>c</sup> Matthew Billing,<sup>b</sup> Andrea Sella<sup>b</sup>

\* Corresponding Author; Email: tom.headen@stfc.ac.uk

## 1 Theory

### 1.1 Data Treatment

The total structure factor  $F(Q)$ , where  $Q$  is the neutron momentum transfer, can be obtained from neutron scattering experiments once corrections have been made for various factors, including but not limited to: background subtraction, multiple scattering, and attenuation.<sup>1</sup> Particular attention needs to be paid to the correction for inelasticity, especially for samples rich in hydrogen. The self-scattering background and effects of inelasticity can be removed from the total differential scattering cross section using an iterative method developed by Soper.<sup>2</sup>

For a system, different but complementary structure factors can be determined for each unique isotopically substituted variant measured. This is especially true for isotopes with large differences in neutron scattering lengths, such as in the case of hydrogen substitution for deuterium  $b_{\text{H}} = -3.74$  fm and  $b_{\text{D}} = 6.67$  fm).<sup>3</sup>

The total structure factor  $F(Q)$  for each sample is equal to the sum of each unique Faber—Ziman partial structure factor  $S_{\alpha\beta}(Q)$ , weighted by the composition and neutron scattering lengths ( $c_{\alpha}$  and  $\bar{b}_{\alpha}$  representing the atomic fraction and average neutron scattering length of atom  $\alpha$  respectively).  $Q$  is the momentum transfer for scattering, equal to  $4\pi \sin \theta / \lambda$ , where  $\theta$  is the angle between the incident and scattered neutron wavevectors and  $\lambda$  the wavelength of the neutron.

$$F_i(Q) = \sum_{\alpha, \beta \geq \alpha} (2 - \delta_{\alpha\beta}) c_{\alpha} c_{\beta} \bar{b}_{\alpha} \bar{b}_{\beta} (S_{\alpha\beta}(Q) - 1) \quad (\dagger 1)$$

The terms concerning the sample composition and neutron scattering lengths can be collected as a matrix of weights  $w_{ij}$ . The sum is again run over all the partial structure factors in the sample.

$$F_i(Q) = \sum_{j=1, N} w_{ij} (S_j(Q) - 1) \quad (\dagger 2)$$

The partial structure factor is related by a Fourier transformation to the partial radial distribution function  $g_{\alpha\beta}(r)$ . This describes the density of  $\beta$  atoms, relative to their bulk density, as a function of distance to  $\alpha$  atoms.  $\rho_0$  is the atomic number density of the sample.

<sup>a</sup> Department of Physics & Astronomy, University College London, Gower Street, London, WC1E 6BT, UK

<sup>b</sup> Department of Chemistry, University College London, 20 Gower Street, London, WC1H 0AJ, UK

<sup>c</sup> ISIS Facility, Rutherford Appleton Laboratory, Chilton, Oxfordshire, OX11 0QX, UK

<sup>d</sup> London Centre for Nanotechnology, University College London, Gower Street, London, WC1E 6BT, UK

$$S_{\alpha\beta}(Q) - 1 = \frac{4\pi\rho_0}{Q} \int_0^\infty r[g_{\alpha\beta}(r) - 1] \sin(Qr) dr \quad (\dagger3)$$

$$g_{\alpha\beta}(r) = \frac{\rho_{\alpha\beta}(r)}{\rho_\beta} \quad (\dagger4)$$

The partial radial distribution function is also related to the cumulative coordination number of  $\beta$  atoms around  $\alpha$  as a function of distance.

$$N_{\alpha\beta}(r) = \int_0^r \rho_\beta g_{\alpha\beta}(r) 4\pi r^2 dr \quad (\dagger5)$$

## 1.2 Empirical Potential Structure Refinement

Empirical Potential Structure Refinement (EPSR) is a method of analysing neutron diffraction data through the use of a Monte—Carlo simulation.<sup>4–6</sup> In short, the simulation is refined against the available scattering data, affording a full 3-dimensional statistical ensemble fully consistent with that data. This box can then be interrogated directly to determine structural and orientational information. Unlike standard RMC methods, which seek to minimise a  $\chi^2$  parameter measuring the ‘goodness of fit’, EPSR aims to minimise the energy of the simulation, as defined by a reference and empirical potential. This has the benefit of helping the simulation avoid getting trapped in local minima on the potential energy surface.

$$U_{\alpha\beta}(r) = U_{\alpha\beta}^{Ref}(r) + U_{\alpha\beta}^{Emp}(r) \quad (\dagger6)$$

The reference potential has a standard form, with the intermolecular part of the potential determined by a Lennard—Jones and a pseudo-Coulombic term (the ‘seed’ parameters), while the intramolecular part is based on harmonic potentials. Through the seed parameters, known information about the system (bond lengths, angles, charges etc.) is included in the simulation, allowing the inclusion of physical parameters into the refinement.

$$U_{\alpha\beta}^{Ref}(r) = 4\epsilon_{\alpha\beta} \left[ \left( \frac{\sigma_{\alpha\beta}}{r_{ij}} \right)^{12} - \left( \frac{\sigma_{\alpha\beta}}{r_{ij}} \right)^6 \right] + \frac{q_\alpha q_\beta}{4\pi\epsilon_0 r_{ij}} \quad (\dagger7)$$

Once the simulation with only the reference potential has equilibrated, the empirical potential is switched on. This potential has a non-standard form, its magnitude varying depending on how poorly the reference potential fits the data at a certain value of  $Q$ .<sup>6</sup> It is used to perturb the simulation box such that the calculated structure factors more closely resemble the actual diffraction data.

The form of the empirical potential is shown in Equations [†8](#) and [†9](#).  $\rho$  is the atomic number density and  $\sigma_r$  a width function, both constant. The potential overall is a series of Poisson functions.<sup>6</sup>

$$U^{EP}(r) = kT \sum_i C_i p_{n_i}(r, \sigma_r) \quad (\dagger8)$$

$$p_n(r, \sigma) = \frac{1}{4\pi\rho\sigma^3(n+2)!} \left( \frac{r}{\sigma} \right)^n \exp \left[ -\frac{r}{\sigma} \right] \quad (\dagger9)$$

For every  $r$  value that falls within the range of the empirical potential (each  $r_i$ , normally spaced by 0.1 Å), a function following that in Equation [†9](#) is generated, using Equation [†10](#).

$$n_i = \frac{r_i}{\sigma_r} - 3 \quad (\dagger10)$$

The magnitude of the empirical potential at an  $r_i$  is represented by the coefficient  $C_i$ . The coefficients are calculated by fitting a series of the Fourier-transformed  $p_n(r, \sigma)$ , shown in Equation [†11](#), to the difference between the data and the simulation in  $Q$  space.

$$P_n(Q, \sigma) = 4\pi\rho \int p_n(r) \exp(iQr) dr = \frac{1}{(n+2)(\sqrt{1+Q^2\sigma^2})^{(n+4)}} \left[ 2\cos(n\alpha) + \frac{(1-Q^2\sigma^2)}{Q\sigma} \sin(n\alpha) \right] \quad (\dagger 11)$$

The coefficients are refined over the course of the simulation to minimise the difference between the simulation and the data (a detailed description of the refinement process is located in [Soper](#)).<sup>6</sup> Due to errors introduced in the data treatment, as well as in the experimental procedure itself, the magnitude of the empirical potential is capped to avoid unphysical structures being introduced to the simulation box.

## References

- [1] H. E. Fischer, A. C. Barnes and P. S. Salmon, *Reports Prog. Phys.*, 2006, **69**, 233–299.
- [2] A. K. Soper, *ISRN Phys. Chem.*, 2013, **2013**, 1–67.
- [3] T. F. Headen, C. a. Howard, N. T. Skipper, M. a. Wilkinson, D. T. Bowron and A. K. Soper, *J. Am. Chem. Soc.*, 2010, **132**, 5735–5742.
- [4] A. Soper, *Chem. Phys.*, 1996, **202**, 295–306.
- [5] A. Soper, *Mol. Phys.*, 2001, **99**, 1503–1516.
- [6] A. K. Soper, *Phys. Rev. B*, 2005, **72**, 104204.

## 2 Figures

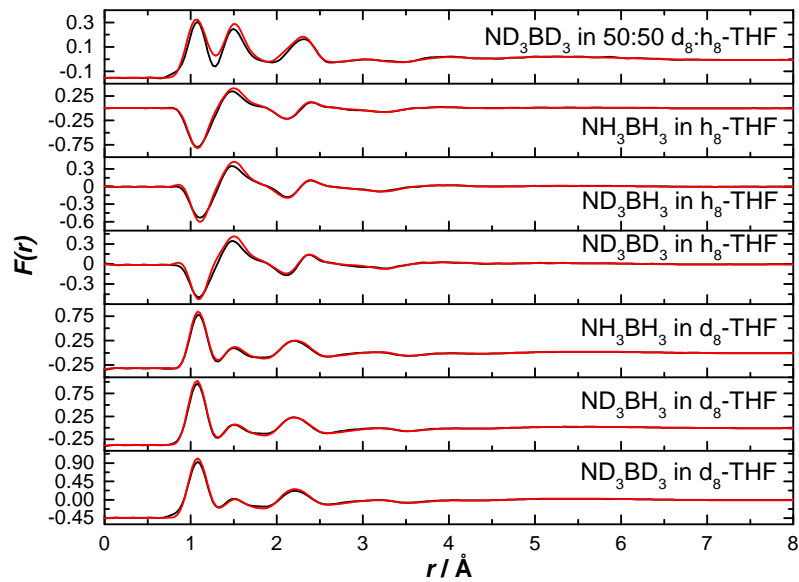


Figure †1: Radial distribution functions from Fourier transformation of the experimental data (black) and the EPSR fitted structure factor (red) for ammonia borane dissolved in THF.

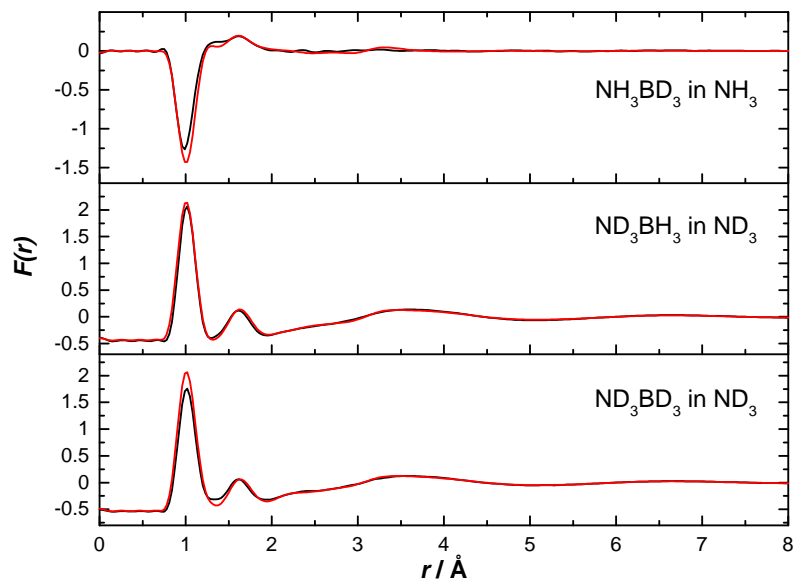


Figure †2: Radial distribution functions from Fourier transformation of the experimental data (black) and the EPSR fitted structure factor (red) for ammonia borane dissolved in ammonia.

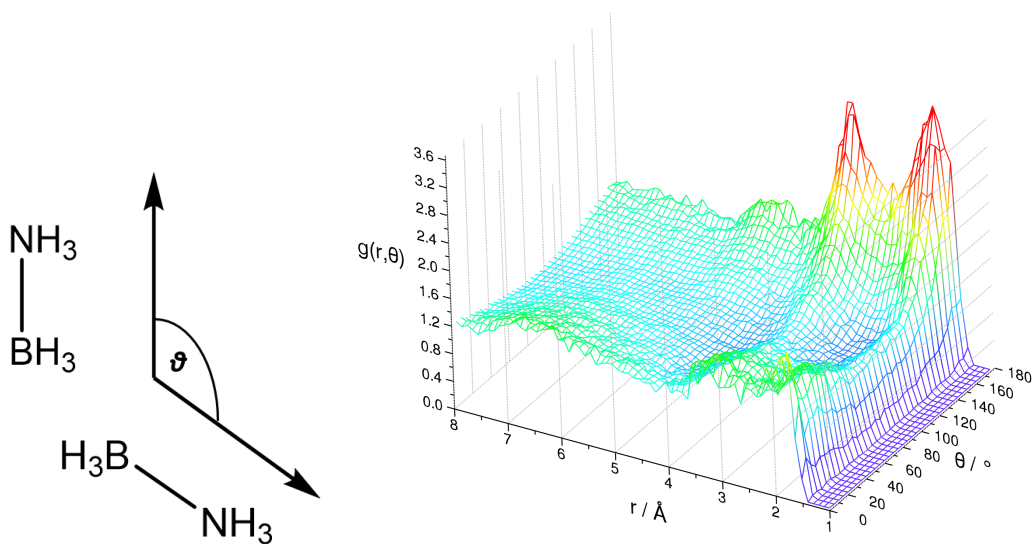


Figure †3: Angular radial distribution function for AB-AB interactions for AB dissolved in ammonia, where  $\theta$  is the angle between the AB dipoles. The distance is that between an  $\text{H}_\text{N}$  and  $\text{H}_\text{B}$ , hence the first peaks show the angles between the dipoles on dihydrogen bonding pairs.

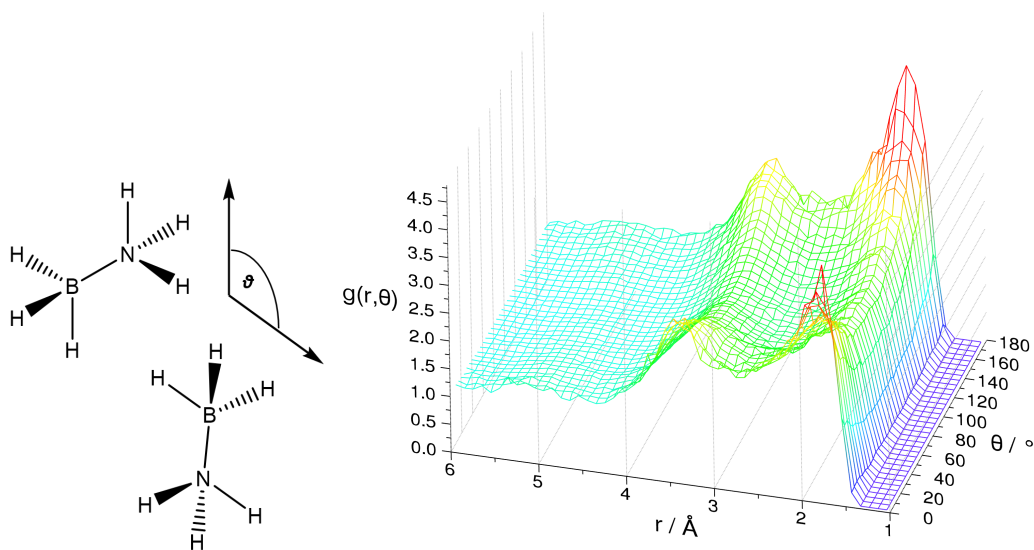


Figure †4: Angular radial distribution function for AB-AB interactions for AB dissolved in THF, where  $\theta$  is the angle between the N-H bonds. The distance is that between an  $\text{H}_\text{N}$  and  $\text{H}_\text{B}$ .

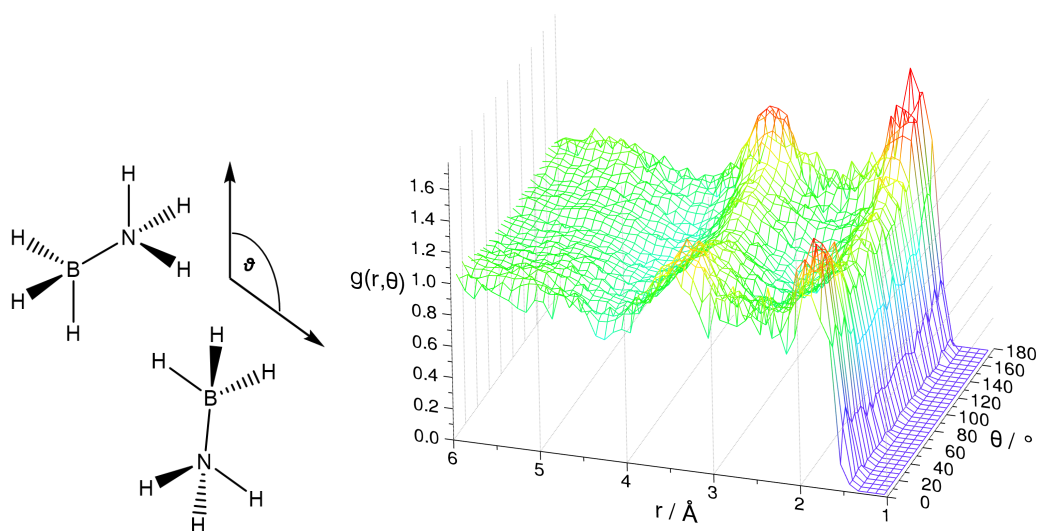


Figure 15: Angular radial distribution function for AB-AB interactions for AB dissolved in ammonia, where  $\theta$  is the angle between N-H bonds. The distance is that between an  $H_N$  and  $H_B$ , hence the first peaks show the angles between N-Hs on dihydrogen bonding pairs.

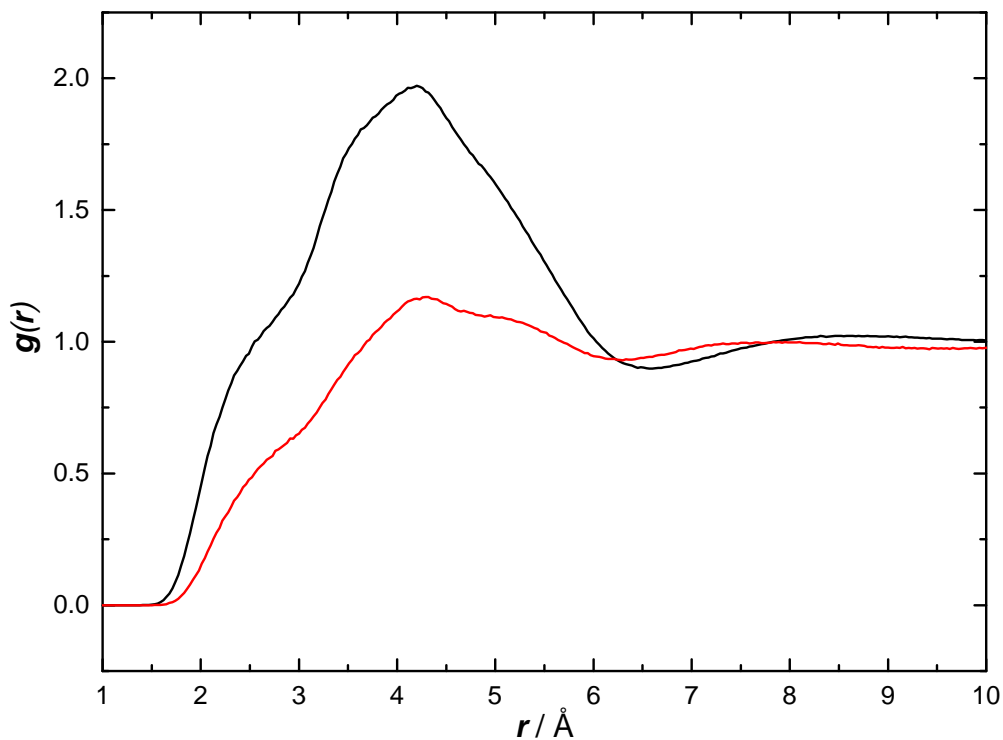


Figure 16: Partial radial distribution functions for  $H_N \cdots H_N$  interactions for the model of AB dissolved in THF (black) and liquid ammonia (red). The first peaks are located at 4.2 Å, indicating that  $H_N \cdots H_N$  dihydrogen bonds do not occur in these systems.

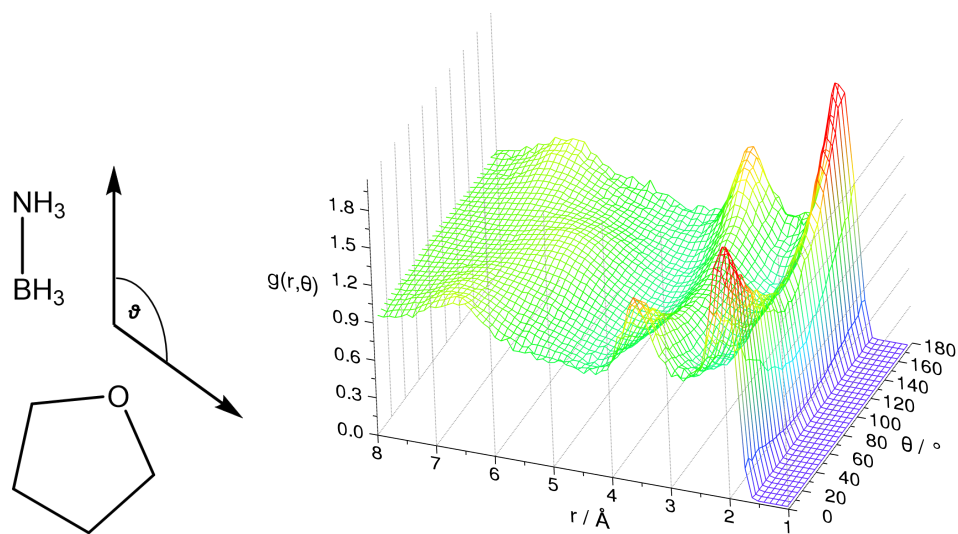


Figure †7: Angular radial distribution function for AB-THF interactions, where  $\theta$  is the angle between the AB dipole and the axis running along the plane of the THF ring, perpendicular to the THF dipole. The distance is that between  $H_N$  and O1. This shows orientations with the THF oxygen pointing at the  $H_N$  rather than parallel to the AB dipole is more favourable.

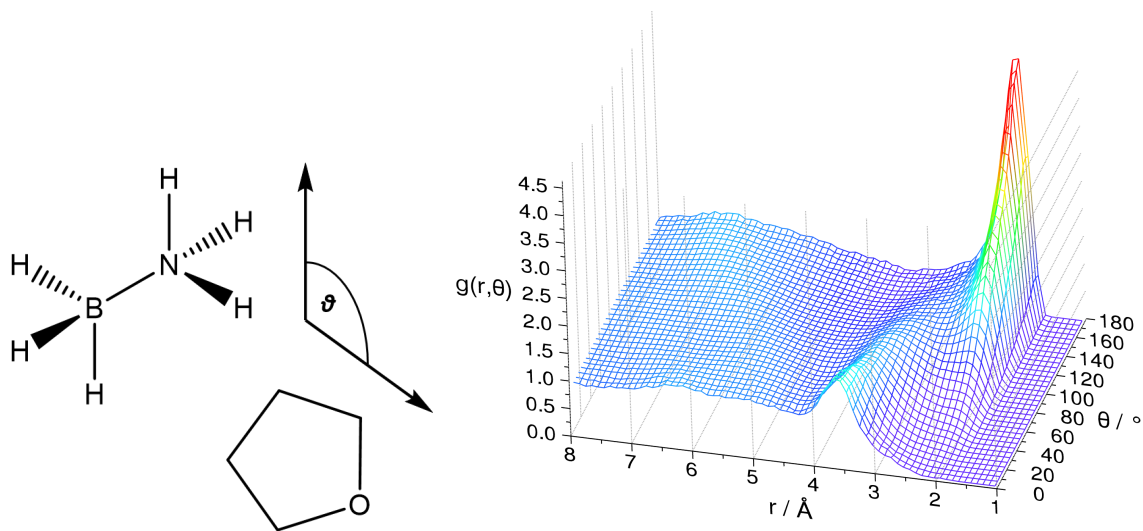


Figure †8: Angular radial distribution function for AB-THF interactions, where  $\theta$  is the angle between an N-H bond and the THF dipole. The distance is that between  $H_N$  and O1. This shows orientations with the THF oxygen pointing at the  $H_N$  rather than parallel to the AB dipole is more favourable.

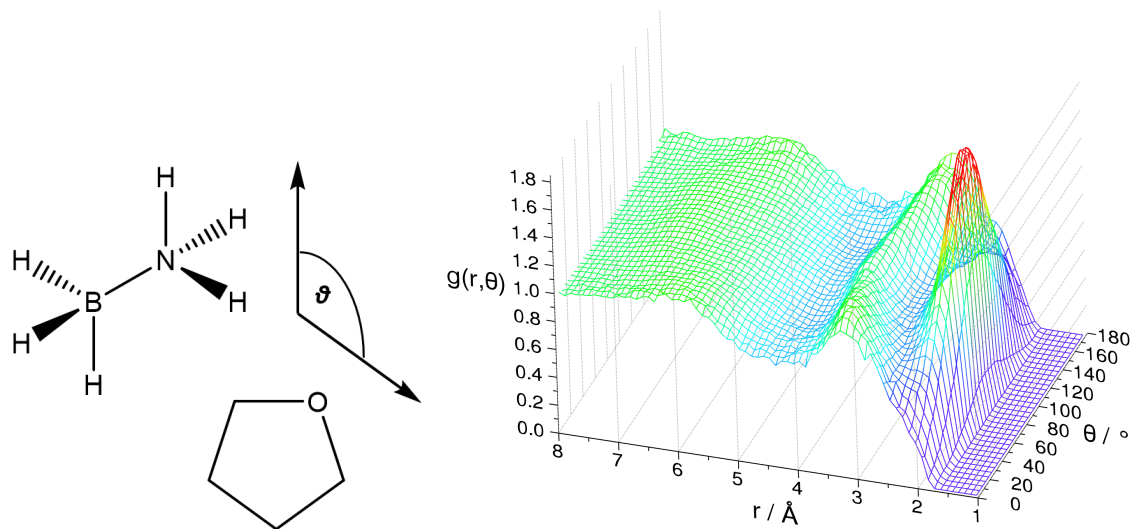


Figure †9: Angular radial distribution function for AB-THF interactions, where  $\theta$  is the angle between an N-H bond and the axis running along the plane of the THF ring, perpendicular to the THF dipole. The distance is that between  $H_N$  and O1. This shows orientations with the THF oxygen pointing at the  $H_N$  rather than parallel to the AB dipole is more favourable.

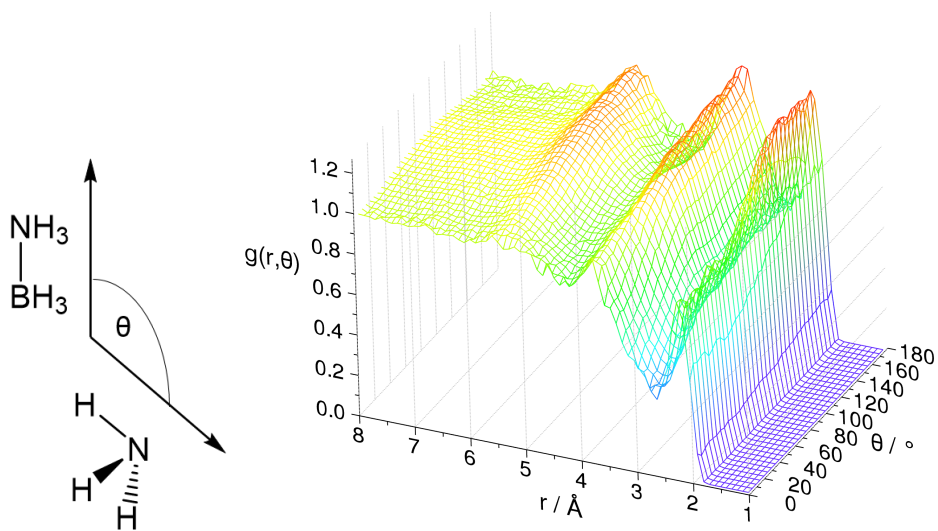


Figure †10: Angular radial distribution function for AB-ammonia interactions, where  $\theta$  is the angle between the AB dipole and an ammonia  $H_A-N_A$  bond. The distance is that between an  $H_N$  and  $N_A$ .

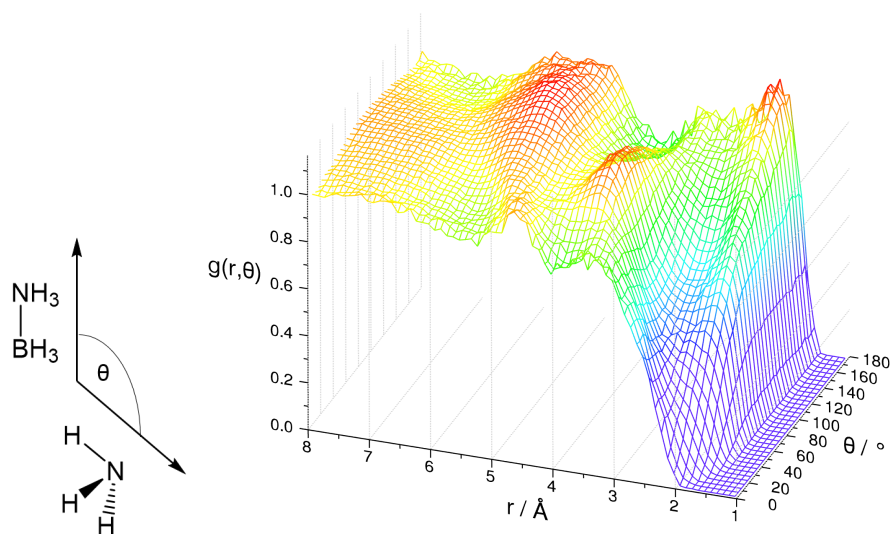


Figure †11: Angular radial distribution functions for AB-ammonia interactions, where  $\theta$  is the angle between the AB dipole and an ammonia  $H_A-N_A$  bond. The distance is that between an  $H_B$  and  $H_A$ .

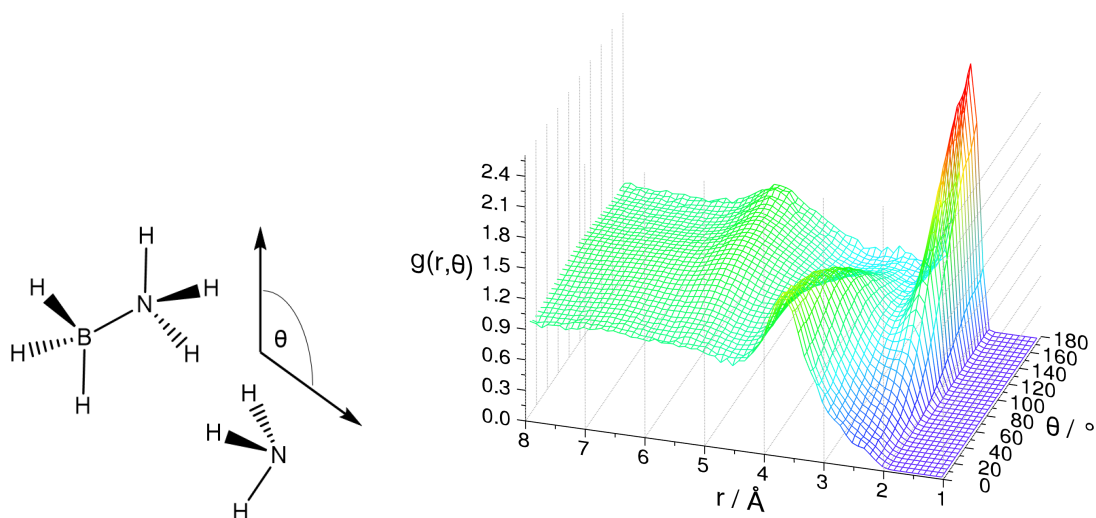


Figure †12: Angular radial distribution function for AB-ammonia interactions, where  $\theta$  is the angle between an AB N-H bond and the plane perpendicular to an ammonia  $H_A-N_A$  bond. The distance is that between an  $H_N$  and  $N_A$ .

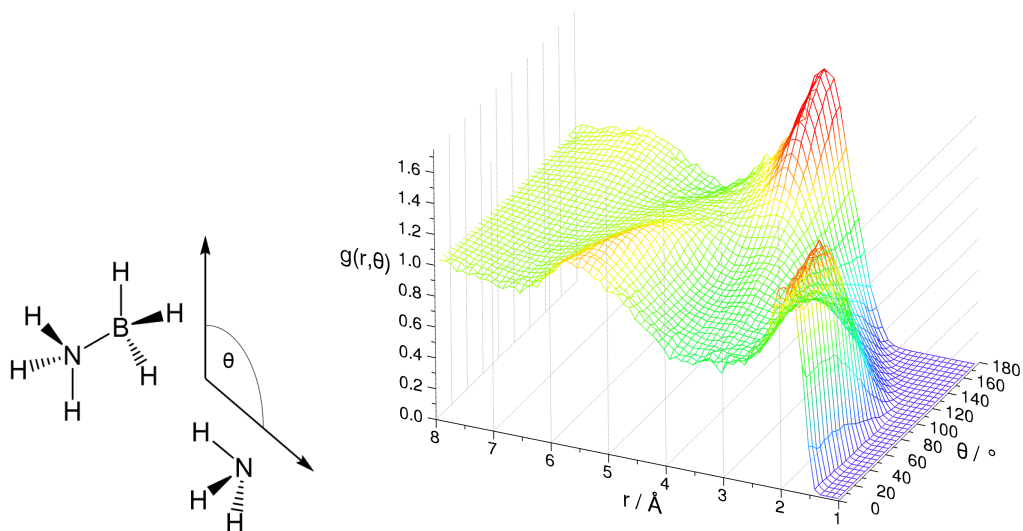


Figure †13: Angular radial distribution function for AB-ammonia interactions, where  $\theta$  is the angle between an AB B-H bond and an ammonia  $H_A-N_A$  bond. The distance is that between an  $H_B$  and  $H_A$ .

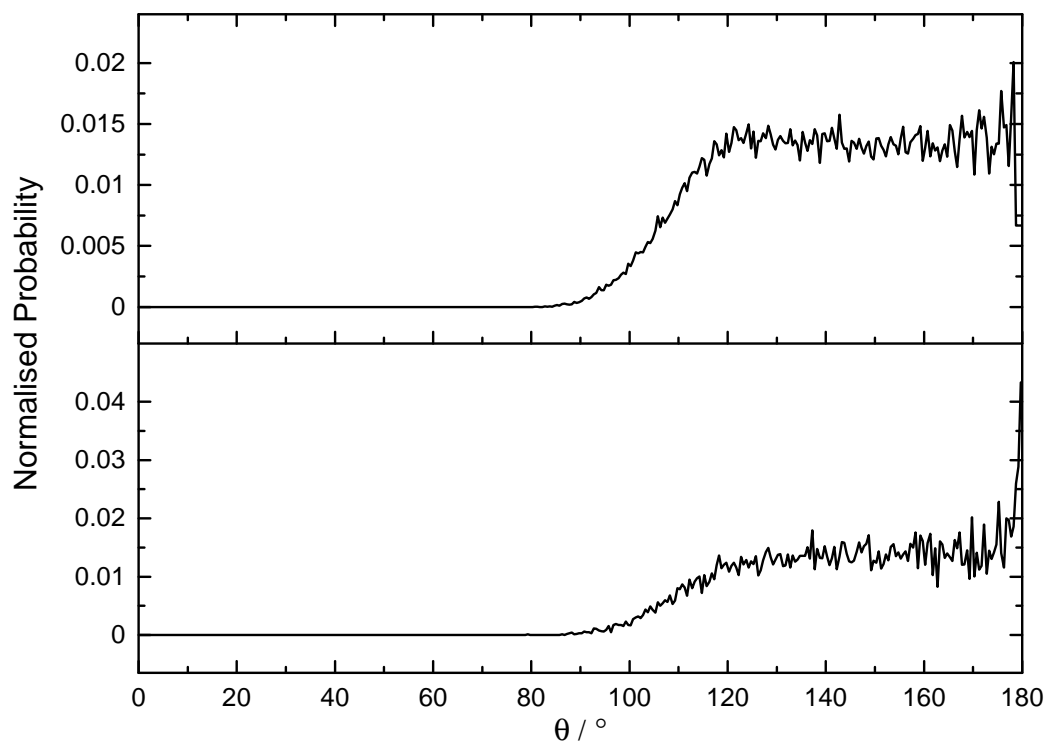


Figure †14: Normalised probability distributions for the angle  $B-H_B \cdots H_B$ , in (top) AB dissolved in THF and (bottom) AB dissolved in liquid ammonia. A maximum  $H_B \cdots H_B$  distance of 2.2 Å was set.